Contents lists available at ScienceDirect

Journal of Nuclear Materials

journal homepage: http://ees.elsevier.com

The effects of impurity gas seeding on the growth of fuzzy tungsten

Patrick McCarthy [a,*], Dogyun Hwangbo [b], Shin Kajita [c], James W. Bradley [a]

[a] Department of Electrical Engineering and Electronics, University of Liverpool,9 Brownlow Hill, Liverpool L69 3GJ, Merseyside, United Kingdom
[b] Faculty of Pure and Applied Sciences, University of Tsukuba, Tsukuba 305-8577, Ibaraki, Japan
[c] Institute of Materials and Systems for Sustainability, Nagoya University, Nagoya 464-8603, Japan

ARTICLE INFO

Article history:
Received 4 December 2020
Received in revised form 30 April 2021
Accepted 29 May 2021
Available online xxx

Keywords
Helium
Tungsten
Fuzzy tungsten

ABSTRACT

Using the linear plasma device NAGDIS-II operating with gas mixtures of helium (He) and impurity (Ne, N_2, Ar), fibre-form nanostructures known as "fuzz" have been grown on tungsten (W) samples. In this system, fuzzy W was grown over a range of sample temperatures and ion fluences (containing He and impurity ion mixtures), but with operator control over the impurity to helium percentage (from 5 – 10%). The ion energies were held constant at 60 eV throughout the experiments. Close inspection of the surface morphologies showed that a variation in fuzzy structure was produced on W surfaces depending on the impurity species used. Specifically, Ne impurity produced cone-like fuzz structures and Ar and N_2 caused more random tendril growth. Using a constant fluence of He and impurity ion species, the effective fuzzy layer growth rate is reduced for higher impurity atomic masses and higher concentrations. For 10 % N_2 within the He plasma, little fuzz growth was visible on the W surface. Where 7.5 – 10% of Ar was used, fuzz growth was terminated completely. From mass loss measurements the net erosion yields of W surfaces exposed to 95 % He + 5% impurity (Ne or N_2) discharges were measured to be lower than bulk W sputtering yields for each impurity species, decreasing sharply with increasing fuzz thickness. Under high ion fluences up to 10^{27} m^{-2}, steady-state thicknesses of W fuzz were attained due to the combined effect of fuzz growth and sputter erosion caused by the impurity species in the plasma. The measured steady-state thicknesses were found to be consistent with an analytical model developed for the simultaneous growth and erosion of fuzz. SEM imaging showed the presence of larger fuzzy structures, Nano-tendril bundles (NTBs), on surfaces where fuzz grew under the presence of impurity species. The formation of NTBs were characterised in terms of their surface temperature threshold ranges.

1. introduction

In the future thermonuclear reactor ITER, tungsten (W) is the proposed material to be used for plasma-facing components (PFCs) due to its high melting point, low sputter rate, and high thermal conductivity [1]. During ITER's operation, helium (He) ash will be produced as a product of the deuterium-tritium (D-T) fusion reaction. It is well known that He bombardment of W can lead to bubble formation beneath the surface region [2], causing plastic deformation and small craters visible on the surface [3]. More recently it has been demonstrated how under certain surface temperatures (1000–2000 K [4]), ion energies (> 25 eV [5]), and He ion fluence conditions (> 10^{24} m^{-2} [6]), He ion irradiation of W surfaces can cause surface nanostructures known as 'fuzz' to grow [7]. Given the expected He ion fluxes (10^{24} m^{-2} s^{-1}), He ion energies (> 10 eV) and W PFC surface temperatures (300–1200 K) [8] within ITER, fuzz is likely to be formed on W.

W fuzz is known to limit the performance of the W surfaces it forms on (the thermal conductivity decreases to 1% [9] and enhanced W fuzz surface erosion is a possibility [10]). This will be of particular concern in the exhaust (divertor) region of the reactor where large power loads (30 MW m^{-2}) and energetic ions (>100 eV) are likely to bombard PFCs [8,11]. If left unmitigated, ions impacting with these energies and power loads would exceed the operational engineering limits of the PFCs (10 MW m^{-2} during steady state and 20 MW m^{-2} during slow transients) [12]. To reduce ion energies and power loads on the PFC materials, impurity gas species will be flowed in front of divertor regions [8,13–15]. The power dissipation involved in this process will be governed by charge exchange and radiation loss processes, with gas impurity seeding known to increase the latter significantly. As a consequence of the radiation losses, the electron temperature is reduced to tens of eV where atomic processes and recombination become significant. The decrease in plasma density in the divertor regions produces a detachment of the divertor region plasma from the core plasma. In preparation for ITER, there have been several tokamak experiments at ASEDX Upgrade (AUG), Alcator C-Mod, DIII-D and JET using various impurity species (e.g., Ne, N_2, Ar) to induce divertor detachment [14,16,17]. Similar impurity species will feature in the future demon-

* Correspondence to: Gencoa Ltd, 4 De Havilland Drive, Liverpol L24 8RN, UK.
E-mail addresses: patrick.mccarthy@gencoa.com (P. McCarthy); j.w.bradley@liv.ac.uk (J.W. Bradley)

https://doi.org/10.1016/j.jnucmat.2021.153125
0022-3115/

stration fusion power plant DEMO [18,19]. Introducing a new gas impurity species into the divertor region also raises concerns for PFC sputtering by these impurities. For extended pulse operations of fusion plasmas, it is vital to limit the concentration of sputtered PFC material within the plasma [20]. A concern for ITER could be the removal of fuzzy W layers due to impurity species sputtering and subsequent poisoning of the fusion plasma.

The dependence of the fuzzy layer thickness, h, on the incident ion fluence, Φ, (given by the product of the constant helium ion flux density Γ_{He} and exposure time t) has been investigated in earlier work [6], and was shown to follow the relationship:

$$h(\Phi) = \left(C\left(\Phi - \Phi_0\right)\right)^{\frac{1}{2}} \quad (1)$$

where Φ_0 is an experimentally determined incubation ion fluence, describing the threshold condition for fuzz formation. The constant C is given by $2D/\Gamma_{He}$, where D is the Fick's law diffusion coefficient for one dimensional material transfer, and is dependent on the sample surface temperature, T_S. Values for C have been calculated for a range of surface temperatures (1120–1400 K) in previous studies [5,21,22]. In practice, Eq. (1) can be used to predict the thickness of a fuzzy layer given the helium ion fluence and surface temperature reached during an experiment. However, the thickness of fuzzy W layers has been shown to decrease where bombarding ionic species have energies exceeding the sputtering threshold on W [23,24]. An extension to Eq. (1) was proposed [6] to account for any surface erosion of the fuzzy layer:

$$h(\Phi) = \frac{C}{2\epsilon_{fuzz}}\left(W\left[-\exp\left(-\frac{2\epsilon_{fuzz}^2}{C}\left(\Phi-\Phi_0\right)-1\right)\right] + 1\right) \quad (2)$$

where ϵ_{fuzz} is an erosion parameter equivalent to an erosion rate (E) divided by the He ion flux (Γ_{He}), and W is the Lambert function. An implication of Eq. (2) is that after some time, the fuzz growth and erosion rate will balance, producing an effective fuzz growth rate of zero. This leads to the formation of a non-changing fuzzy layer or steady-state thickness. Observations of this steady-state thickness have been made in previous studies [6,23,24]. In the case of ITER, fuzzy W can form in areas where high fluxes of impurity ions are likely to bombard the surface [8]. Understanding the interplay between these mixtures of He and impurity ion fluxes on W surfaces and any subsequent fuzz growth is therefore an area of interest for the performance of PFCs within fusion reactors.

In this study, He discharges combined with different gas impurities (N_2, Ne, or Ar) are exposed to W surfaces within the linear plasma device NAGDIS-II. NAGDIS-II is a device capable of reproducing the plasma conditions (plasma density, electron temperature) expected for the ITER divertor. In the experiments made in this study, the impurity levels were set at 5, 7.5, and 10%, with bombarding ion energies maintained at 60 eV and W surface temperatures in the range 1320–1550 K. The surface temperatures, ion energies, and impurity species were chosen to be consistent with those expected for the ITER divertor [8,14]. Surface characterisation of the fuzzy W layers is used to analyse the effect of the impurity percentage and total ion fluence on the fuzz growth, namely the surface morphologies produced, mass loss, optical reflectivity, and fuzzy layer thickness.

2. Experimental arrangement

2.1. The plasma rig: NAGDIS-II

The linear magnetised plasma device NAGDIS-II (NAGoya DIvertor Simulator II) was used to produce fuzzy tungsten samples grown under concurrent He and impurity ion irradiation [25]. It consists of a high density helium plasma arc injected in a 0.1 T axial magnetic field. Langmuir probe measurements revealed typical electron density and temperature values of ~ 10^{19} m^{-3} and ≈ 5 eV respectively. The incident ion flux was calculated to be in the range of 2.5×10^{21} to 2×10^{22} m^{-2} s^{-1} and over the time intervals used in this study, He + impurity fluences corresponded to 2×10^{25} to 2×10^{27} m^{-2}.

Square sheets of W (purity 99.95 % supplied by PLANSEE) 10 mm long and 0.2 mm thick were suspended on a conducting rod ≈ 1.4 m downstream of the plasma source. W samples were biased negatively, using a DC power supply, to maintain an incident ion energy of 60 eV, taking into account the plasma potential (- 5 V). The surface normal of each sample was oriented at a 45° angle to the magnetic field lines, allowing a temperature measurement via an infra-red pyrometer (KTL-PRO), sensitive to 1.6 μm wavelengths, to be made. The emissivity of the W surface was taken to be 0.3 at the 1.6 μm wavelength. At the start of the plasma exposure, assuming at this point no fuzz had begun to grow, the surface temperature was measured. It was determined that the initial temperature of the W surface would be used to represent the surface temperature (T_S) in this study. The surface temperatures were measured to be in the range 1320 – 1500 K. It is important to note that as the plasma exposure time increased, the W surfaces become optically black (due to fuzz growth). The emissivity of the surface will increase and the measured surface temperature will decrease gradually [26].

The base pressure of the system was on the order 1×10^{-5} Pa and maintained by two turbo molecular pumps (TG 200M Osaka Vacuum Ltd), backed by rotary pumps and measured by a capacitance manometer gauge (Type 627 MKS Instruments). The He gas was supplied to the source region, whilst the impurity species of N_2, Ar or Ne were introduced to the downstream end of the device. All gases were regulated using a mass flow controller (HORIBA STEC), and measured using a capacitance manometer gauge (Type 627 MKS Instruments) located in the downstream region of the sample position. With low base pressures and operating pressures between 0.6 – 0.7 Pa, any background impurity (residual air) could be ignored when considering the composition of the plasma species. To fix the percentage levels (i.e 5, 7.5 and 10 %) of the chosen impurities, He gas was first introduced into the system to a known pressure. Shortly afterwards the impurity gas was added until the required pressure increase was reached indicating the desired quantities of each in the system.

In each case where an impurity percentage was estimated, the ionisation energy for each gas present in the plasma was not accounted for in the results of the ion flux or fluence. This may lead to an under estimation of the species percentage within the plasma; the first ionisation energies of Ne (22 eV [27]), Ar (16 eV [28]) and N_2 (15 eV [29]) are all less than that of He (25 eV [30]), implying a different rate of ionisation may occur for each gas species mixture. The ratio of impurity (Ne, N_2, Ar) ions to He ions is also unlikely to equal the impurity/He gas ratio due to Penning ionisation of impurity species via He metastable states [31].

2.2. Fuzzy tungsten surface analysis

Surface microscopy was performed on W fuzz samples using two different scanning electron microscopes (SEMs); one a JEOL 7001F Schottky field emission SEM and the other a FEI Helios Nanolab 600i focused ion beam scanning electron microscope (FIB-SEM). The fuzzy W layer thickness was measured by mechanically fracturing each sample, allowing the cross section of the sample to be viewed. An average of 100 thickness measurements was taken, with the specified error equivalent to twice the standard deviation. The optical (specular) reflectivity of each surface was measured using the USB2000 + spectrometer (Ocean Optics) and corresponding DH-2000-BAL deuterium halogen light source. The measurement of the reflectivity at a wave-

length of 632.8 nm was taken for the comparison between fuzzy W samples as per previous studies on fuzzy W reflectivity [32,33]. Energy dispersive x-ray (EDX) analysis was used to identify the elements present in a W fuzz sample. The Helios Nanolab 600i FIB/SEM was equipped with an EDAX Octane Pro EDX detector, and the acquired spectra were analysed using the EDAX EBSD DigiView with integrated EBSD EDS TEAM analysis software.

2.3. Mass loss measurements and determination of net erosion yields

With the presence of impurities in the He plasma and the ion energy that was chosen for the experiments (ions had an energy of 60 eV - above the sputtering threshold of N_2, Ne and Ar on W), some level of sputtering of the W samples during plasma exposure was expected. To quantify this, mass measurements were made pre and post plasma irradiation using an A & D Co. BM-22 microbalance, with a precision of 1 μg. The mass of each W sample was recorded 20 times (both pre and post irradiation) and from this an average mass loss value Δm was found. Based on this mass loss Δm, the net erosion yield Y_{fuzz} of a fuzzy W surface due to He-impurity plasma irradiation was calculated using the equation [34],

$$Y_{fuzz} = \frac{\Delta m}{A \Phi m_W} \tag{3}$$

where A is the area of the sample, Φ is the fluence of particles to the sample surface and m_W is the mass of a W atom.

2.4. Sample porosity measurements

The porosity of plasma exposed fuzzy W samples was calculated using a similar technique to that given by Doerner et al. [35,36]. In their method, the surface fuzz is removed by wiping the surface, the resultant mass loss and volume of the removed layer are then calculated. The mass measurements were made using a XS205DU analytical balance manufactured by Mettler Toledo with a precision of 10 μg. In each case the mass of the sample was measured 10 times before and after the fuzzy W layer was removed. Fuzzy layers were removed by wiping with a paper cloth, and SEM imaging was used to show the layer of fuzz had been removed. Explicitly the porosity of the fuzzy layer p_{fuzz} is given as [37],

$$p_{fuzz} = 1 - \frac{\Delta m_{fuzz}}{\rho_W V_{fuzz}} \tag{4}$$

where, Δm_{fuzz} is the measured mass difference between and after the fuzz removal, ρ_W is the bulk W density and V_{fuzz} is the volume of fuzz removed.

2.5. Analytical model describing fuzzy tungsten growth in erosive plasmas

In the absence of any surface erosion the thickness h of the growing fuzzy W layer can be described by Eq. (1). In the presence of impurity ions in the plasma or very high He bombarding energies, the fuzzy layer thickness can be reduced by physical sputtering. In this case, Eq. (1) is modified by inclusion of an erosion parameter ϵ_{fuzz} to give Eq. (2).

The erosion parameter ϵ_{fuzz} is related to the bulk sputtering yield of a surface, Y_{bulk}, by,

$$\epsilon_{fuzz} = \frac{Y_{bulk} m_W}{\rho_W} \tag{5}$$

where m_W and ρ_W are the atomic mass and density of bulk W respectively. Following the work in [6,24,37], the parameters in Eq. (5) can be calculated using experimentally measured net erosion yields, Y_{fuzz}, but the porosity, p_{fuzz}, of the fuzzy surface must also be considered. In this way, Y_{fuzz} relative to Y_{bulk} varies by the term (1 - p_{fuzz}), i.e $Y_{fuzz} \approx (1 - p_{fuzz}) Y_{bulk}$. Therefore, in the case where Y_{fuzz} is used, the erosion parameter is now represented by,

$$\epsilon_{fuzz} = \frac{Y_{fuzz} m_W}{\rho_W \left(1 - p_{fuzz}\right)} \tag{6}$$

Inspection of Eq. (2) and using the properties of the Lambert function [38] shows that for ever-increasing fluences ($\Phi \rightarrow \infty$) the fuzz layer thickness tends to a value of h ($\Phi \rightarrow \infty$) given by $C/2\epsilon_{fuzz}$. This value can be calculated and indicates an estimation for the steady-state thickness (h^{ss}) of fuzz, a stage in the formation of fuzzy W where the growth and erosion rates are equal. By substitution of Eqs. (5) and (6) in to the limit of the steady-state thickness $C/2\epsilon_{fuzz}$, h^{ss} is given as,

$$h_{ss} = C \left(\frac{\rho_w}{2 m_w Y_{bulk}} \right) \tag{7}$$

$$h_{ss} = C \left(\frac{\rho_w \left(1 - p_{fuzz}\right)}{2 m_w Y_{fuzz}} \right) \tag{8}$$

3. Results

A series of experiments have been performed in which W surfaces were exposed to He + impurity plasma bombardment with a variation of operation conditions. These were discharges containing He and small concentrations (5, 7.5 and 10 %) of Ne, Ar or N_2. The typical sample temperatures (T_s) were in the range 1320 to 1500 K, with incident ion energies of 60 eV, and the operating pressure in the range 0.6 – 0.7 Pa. Samples were exposed to He + impurity plasmas for increasing amounts of time, providing ion fluence (Φ) ranges of 5×10^{24} to 2×10^{27} m^{-2}. After plasma exposure, the samples were analysed by SEM to provide fuzz thickness measurements (h) and images of the surface morphologies produced. In addition to the surface microscopy, mass loss, optical reflectivity and porosity measurements were made.

3.1. Surface morphologies

Initially, ten samples of W were exposed to He + impurity plasma within NAGDIS-II to an ion fluence of $\approx 5 \times 10^{25}$ m^{-2}, for increasing percentages of impurity (from 5% to 10 %). The ion energy was maintained at 60 eV and T_s was in the range 1320 to 1500 K. In Fig. 1, the cross-sectional thickness (top row) and surface morphologies (bottom row) are imaged for W surfaces exposed to plasmas containing 100 % He (a) & e)), 95 % He + 5 % Ne (b) & f)), 95 % He + 5 % N_2 (c) & g)), and 95 % He + 5 % Ar (d) & h)). Where the surface morphologies (bottom row of Fig. 1) are imaged, samples were tilted to 45° from the surface normal. It is clear from the images that with the introduction of a small amount of impurity into the He plasma, the thickness of the fuzzy W layer is reduced. A factor of 2 reduction in the thickness was observed for Ne impurity, and a factor of 3 reduction in thickness was observed for the N_2 and Ar impurity, compared to the case of pure He irradiation. There are also some changes in morphology observed, for instance with 5 % of Ne impurity where the surface structures appear to be more cone-like than tendril. Similar cone-like nanostructures were seen in a separate report where heated W surfaces were exposed to a He + Ne plasma mixture [39]. The effect of impurity on fuzzy W growth can be seen more readily for higher concentrations of impurity as shown in Fig. 2. The cross sectional and tilted images reveal that with 10 % impurity level, fuzzy W growth can be impeded if not almost terminated for higher atomic mass gases (N_2, Ar). This finding agrees well with the observations in a separate report [40] where little fuzz growth was observed when tungsten surfaces were exposed to 90 %

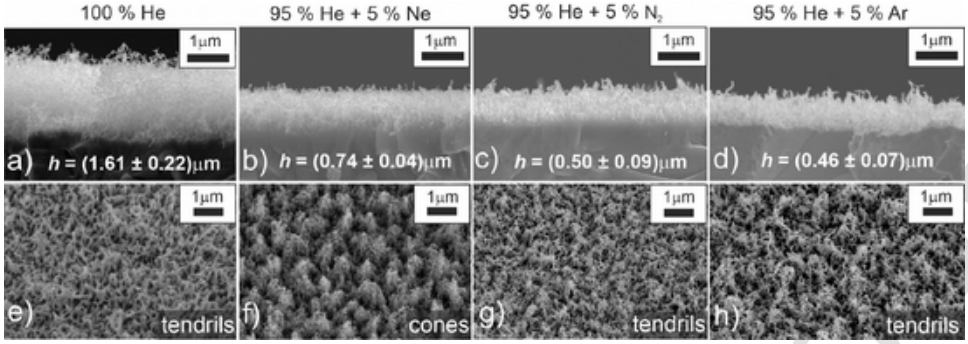

Fig. 1. Cross-sectional SEM micrographs of irradiated samples (top row) and 45 ◦ tilted images (bottom row) for plasmas containing a) and e) 100 % He, b) and f) 95 % + 5 % Ne, c) and g) 95 % + 5 % N_2, and d) and h) 95 % + 5 % Ar. The surface temperature T_s was in the range 1320–1465 K. The ion energy and fluence were 60 eV and ≈ 5×10^{25} m^{-2} (corresponding to 3600 seconds exposure) respectively.

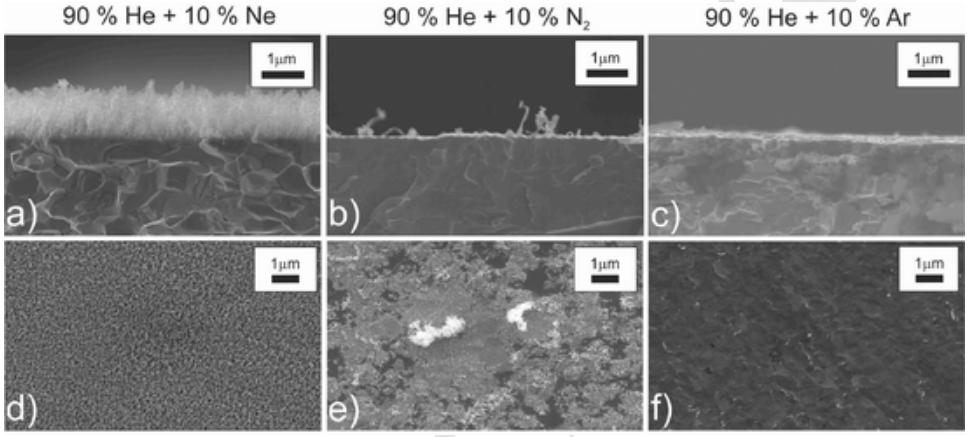

Fig. 2. SEM micrographs similar to those in figure 2 but for 10% impurity levels. The bombarding ion energy and fluences were 60 eV and ≈ 5×10^{25} m^{-2} (3600 s exposure) with T_s between 1320 and 1465 K.

He + 10 % Ar plasma, at similar ion energies, fluences and surface temperatures to the current study.

3.2. Mass loss and optical reflectivity

To understand the trends in Fig. 2 it was useful to measure the mass loss of each sample after irradiation, indicating the level of material erosion due to physical sputtering. Fig. 3 shows the mass loss for the nine different combinations of impurity species and their concentrations, for a fluence of ≈ 5×10^{25} m^{-2} and ion energy of 60 eV. The mass loss of the sample is seen to increase with increasing impurity atomic mass and concentration demonstrating that sputtering is most likely the cause. Fig. 3 also shows a near linear dependence between the mass and impurity concentration and implies, from an extrapolation of the data back to the x-axis (level of impurity %) that there may be a threshold impurity level below which erosion does not occur. It was observed that where the highest percentage of impurity was used (10%), W surfaces treated with N_2 and Ar had little fuzzy nanostructure growth on the surface, and still remained reflective to the naked eye. It was beneficial therefore to quantify the reflectivity of each surface. Fig. 4 shows the measured percentage reflectivity over a range of ion fluences, species, and impurity concentration in the plasma. There is little variation over the range of parameters, with most fuzzy W samples showing 1–2 % reflectivity, agreeing well with previous reflectivity measurements for fuzzy W layers of similar thicknesses [26,33,41]. However, surfaces experiencing the highest mass loss (plasmas containing 10% of N_2 and 7.5% to 10% of Ar impurities) and little fuzz growth were significantly more reflective (4–16 %) than those with lower mass losses and typical fuzz growth on their surface (reflectivity of ≈ 1–2 %).

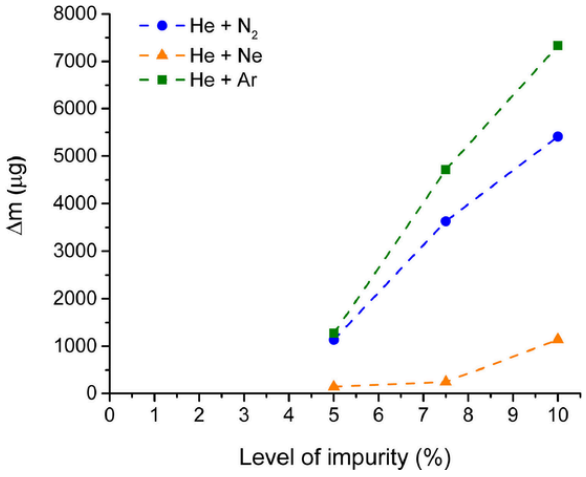

Fig. 3. A plot of the mass loss Δm versus the relative level of impurity for Ne, N_2 and Ar in the He plasma. The bombarding ion energy and fluences were 60 eV and ≈ 5×10^{25} m^{-2} (3600 s exposure) with T_s between 1320 – 1500 K. Errors in Δm were fixed at ≈ 20 μg for each measurement.

3.3. Measured net erosion yields

A further ten W samples were exposed to 95 % He + 5 % impurity (N_2 and Ne) discharges inside NAGDIS-II, with the exposure times increased gradually for each sample to produce a range of fluences of exposure (between $\times 10^{25}$ – 10^{27} m^{-2}). The ion energy was maintained at

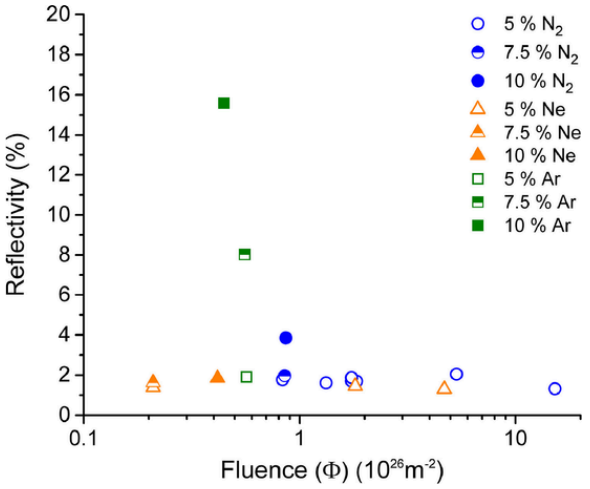

Fig. 4. Reflectivity measurements of fuzzy W surfaces grown over a range of He + impurity ion fluence and impurity percentages. Labels are as shown in the legend (circles for N_2, triangles for Ne and squares for Ar).

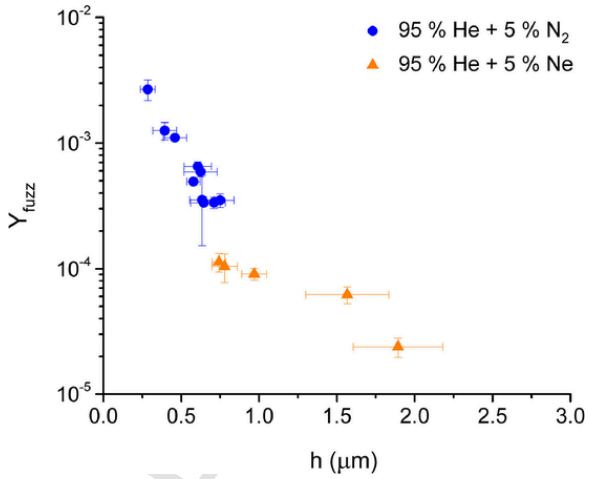

Fig. 5. The net erosion yields against fuzz thickness for 5 % of N_2 and Ne impurity species in a He plasma.

60 eV, and T_s was measured to be in the range 1320 – 1465 K. Each sample was analysed using the SEM to determine the thickness of fuzz that had grown on each surface.

Fuzzy W surfaces have been shown to produce a lower sputtering yield relative to pure W surfaces (i.e. surfaces where no fuzz is present) [37,42,43]. Here the fuzzy surfaces produced with 5 % impurities (N_2 or Ne) are analysed for their experimental net erosion yield and compared with bulk sputtering yields for W under Ne or N_2 ion bombardment [44]. Where N_2 impurities are used in plasma, it has been shown that molecular sputtering can enhance the sputtering yields of surfaces when the incident ion energy is low (< 1 keV) [45,46], even producing 4x larger sputtering yields when the ion energies are ≈ 50 eV [46]. As a similar ion energy (60 eV) is used here, it could be assumed that the yield may be enhanced for sputtering with N_2, therefore bulk sputtering yields for N on W given in [44] were quadrupled when comparing with net erosion yields (Y_{fuzz}). In light of this, the bulk sputtering yield for N_2 on W ($Y_{bulk,N2}$) would now be closer to 3.89×10^{-3}. In the case of Ne, the bulk sputtering yield ($Y_{bulk,Ne}$) given in [44] was reduced by a factor of three in line with the known discrepancy that exists for low mass species bombardments in high flux experiments [47], and taken to be ≈ 1×10^{-3}. To verify this assumption, a pristine W sample was treated with a pure Ne plasma for an ion fluence of 5×10^{24} m^{-2} within NAGDIS-II. After the plasma exposure, the mass change of the sample resulted in a net erosion yield of ≈ 1.3×10^{-3}, a factor of three lower than the theoretical yields predicted in [44], and agreeing well with the findings in [47].

In Fig. 5, the values for Y_{fuzz} calculated for 95 % He + 5 % impurity (N_2 and Ne) discharges are shown against the respective fuzzy W layer thickness (h). It is clear from the results that Y_{fuzz} decreases as h increases. A comparison between Y_{fuzz} values in Fig. 5 and $Y_{bulk,Ne}$ and $Y_{bulk,N2}$ (taken to be 1.3×10^{-3} and 3.89×10^{-3} respectively) shows that for 5% of each impurity, Ne and N_2, the measured net erosion yields were less than their respective theoretical bulk sputtering yields.

3.4. Steady-state thickness measurements from tungsten surfaces

The fuzzy W layers produced under 95 % + 5% impurity (N_2, Ne) plasma exposures were further analysed for their development of a steady-state thickness (h_{ss}) of fuzz, a process known to occur due to the balance of growth and erosion in erosive He plasmas [6]. Eqs. (7) and (8) presented in Section 2.5 allow predictions for the value of h_{ss} to be made, given certain experimental parameters (P_{fuzz} and C) are known.

A 100 % He discharge was used to grow fuzzy W samples and allow the calculation of a temperature constant C at 1465 K; values for C had been previously calculated in the literature to be 8×10^{-38} m^4 at T_s = 1320 K [5]. For T_s = 1465 K, W fuzz samples were produced within NAGDIS-II with their fuzz thicknesses h measured using SEM and plotted on Fig. 6 using black circles. The measured values for h were then used with Eq. (1) to calculate a temperature constant C which best represents the data. Here Φ_0 is estimated to be 5×10^{24} m^{-2} in the calculation of C, giving a good fit to the experimental data for a 100 % He plasma exposure shown in Fig. 6. This estimate of Φ_0 is consistent with previous investigations on NAGDIS-II which have observed an incubation fluence of ≈ 4×10^{24} m^{-2} is necessary for fuzz formation [21]. An average of the C values calculated for each fuzzy layer thickness produced in a 100 % He plasma was made; C at 1465 K was found to be 1.15×10^{-37} m^4. In Table 1, values for C over a range of T_s (1120 – 1465 K) are presented. Values for C are observed to increase given increases in T_s. This increase in the growth rate as the W surface temperature increases has been seen in other studies where fuzzy W layers were measured over increasing surface temperature ranges [5,22].

Eq. (1) is represented as the black dashed line on Fig. 6. A good agreement between the fuzzy W thicknesses grown in 100 % He and the predicted trend of growth given by Eq. (1) is found. The porosity of two layers, produced for the largest fluence samples under 95 % He + 5 % of N_2 or Ne impurity, were measured from the mass before and after the removal of the fuzzy layer, following the procedures given in

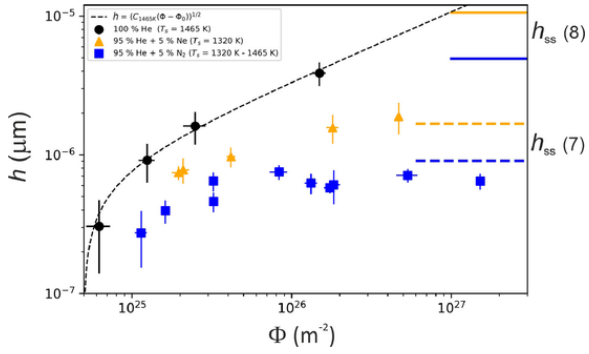

Fig. 6. The W fuzz thicknesses produced in a 100 % He plasma (black points), 95 % He + 5 % N_2 plasma (blue squares) and 95 % He + 5 % Ne plasma (yellow triangles). The horizontal dashed lines represent the steady-state thickness calculated using Eq. (7) for N_2 (blue dashed) and Ne (yellow dashed). The horizontal solid lines show the results of Eq. (8) using the calculated net erosion yield and porosity values for both N_2 (solid blue) and Ne (solid yellow).

Table 1
Comparison of temperature constants C calculated at a range of temperatures, available from the literature and found in the current work.

T_s (K)	Temperature Constant C (m^4)
1120 [5]	2.64×10^{-38}
1320 [5]	8×10^{-38}
1465 (current work)	1.15×10^{-37}

[37]. In Fig. 7, the fuzzy surface of a sample exposed to 95 % He + 5 % N_2 is shown with 50 % of its surface area removed, and cross sectional SEM imaging shows the near total reduction in the fuzzy layer thickness after removal. Where fuzz has been wiped off, there is a chance that the fuzz layer was merely compressed during the process, something that has been observed in other studies where porosity of fuzz was established using the same method [36]. After the fuzzy layer was believed to be fully removed, a mass loss of ≈ 100 μg and ≈ 340 μg was measured for the 5 % N_2 and Ne samples respectively. This corresponded to a porosity of ≈ 0.7 for the fuzzy layer produced under 5 % N_2 (h = 0.65 μm), and 0.9 for the fuzzy layer produced under 5 % Ne (h = 1.89 μm). Now the fuzz thicknesses produced on W samples using He and impurity plasma for a range of fluences will be considered. The measurements of h produced under ion fluences (Φ) of 95 % He + 5% impurity (N_2 or Ne) are shown in Fig. 6. In both cases (N_2 and Ne) the presence of impurity now reduces h relative to the 100 % He case. It is worth noting that the data for 5 % Ne in Fig. 6 were taken at T_s = 1320 K, which would result in a lower temperature constant C, equivalent to 8×10^{-38} m^4 (calculated using data given in [5]). This lower value of C will in turn mean the expected trend of Eq. (1) at 1320 K will be different, however it was found that the presence of 5 % Ne still results in a lower growth rate of fuzz compared to 100% He when this calculation is made.

Comparing the trend of the growth of fuzz for each different impurity in Fig. 6, the heavier atomic mass impurity (N_2) leads to lower effective fuzz growth rates compared to the lower atomic mass impurity (Ne). Specifically the highest fluence samples for the 5 % Ne and N_2 discharges in Fig. 6 show a reduction in h of around 3 times from Ne to N_2. It is likely that this is due to an increased sputtering effect of N_2 compared to Ne, and this agrees with the results in Fig. 3 where an enhancement in mass loss was seen when comparing the one hour discharges containing 5 % Ne or N_2. In addition, the initial surface temperature could also have had an effect on the sputtering yield and subsequent effective fuzz growth rate. T_s was close to 1465 K for some samples produced with 5 % N_2, which is hotter than the surfaces where Ne was used as the impurity during irradiation (T_s = 1320 K). It is has been shown in previous investigations that an increased erosion rate can occur for higher surface temperatures [48], similar effects may have occurred here.

Overall, the thickness of fuzzy layers grown in plasma where impurity is present are reduced relative to the 100 % He case over the fluence range given in Fig. 6.

It is noticeable that the measured h values no longer changes as rapidly as Φ increases, particularly in the case of N_2 where h is very similar above 8×10^{25} m^{-2}. Presumably this is where a balance has been reached between growth and erosion of the fuzz, resulting in a steady-state fuzz thickness [6,23,24]. Now, using the equations introduced in Section 2.5, a calculation for the steady-state thickness (h_{ss}) based on bulk sputtering values of W using Ne ($Y^{bulk,Ne} = 1.3 \times 10^{-3}$) and N_2 ($Y^{bulk,N2} = 3.89 \times 10^{-3}$), or using experimentally determined values for p and Y^{fuzz}, could be made.

Plotted on Fig. 6 are the values for h_{ss} using Eq. (8) (represented with a solid horizontal line) and Eq. (7) (plotted as a longer, dashed line). Greater agreement between results of the irradiations from NAGDIS-II and the predictions of the analytical model is found when bulk sputtering yields are used. The largest discrepancy between the analytical model described in Section 2.5 and the experimental data was seen when using net erosion yields and porosity measurements to estimate h_{ss}. The predicted h_{ss} values for both N_2 (solid blue line) and Ne (solid yellow line) are both much greater than the apparent steady-state thicknesses from the raw data in Fig. 6. It has been mentioned in [6] that a better accuracy in the prediction of fuzz thicknesses is found when using bulk yields over measured net erosion and porosity values, which appears to be the case here.

3.5. Nano-tendril bundle growth

SEM imaging of the fuzzy W surfaces also showed much larger nanostructures than typical fuzzy W morphologies. These larger nanostructures did not show any uniformity in their shape or distribution across the surface, but they were, in some cases, as much as 20 times thicker (≈ 20 μm) than the typical fuzzy W growth observed on the surface. The diameter of the tendrils of these structures were on the order of tens of nm, resembling similar larger fuzz growths known as nano-tendril bundles (NTBs) reported by Woller et al. [49,50] and Hwangbo et al. [39,51].

In Fig. 8, examples of the NTBs on the W surfaces exposed to He + N_2 plasma observed through SEM imaging are shown. In Fig. 8 a)–c), the NTBs were produced after treatment with 92.5 % He + 7.5 % N_2 plasma for an ion fluence of 6×10^{25} m^{-2}. In Fig. 8 d) and e) NTBs were formed after exposure to a plasma with 90 % He + 10 % N_2 for an ion fluence 8×10^{25} m^{-2}. The NTBs were observed to be near randomly distributed across the surface, with their average height difficult to measure due to the large quantity of NTBs that were observed to have formed. An attempt was made to use a focused ion beam to mill a cross section of selected NTBs, but due to the onset of melting (presumably due to the ion current used in the milling) this was abandoned.

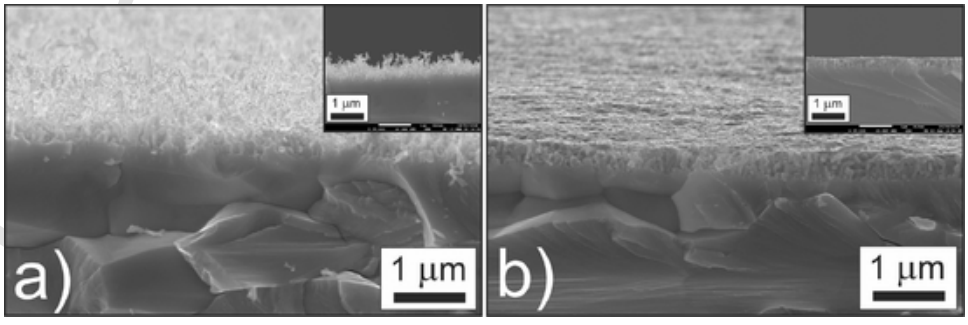

Fig. 7. SEM images of the fuzzy W surface grown under 95% He + 5% N_2 plasma for an ion fluence of 1.5×10^{27} m^{-2}, with the surface before (a) and after (b) removal of the fuzzy layer. Inset is a cross-sectional SEM image of the fuzzy layer pre and post wiping.

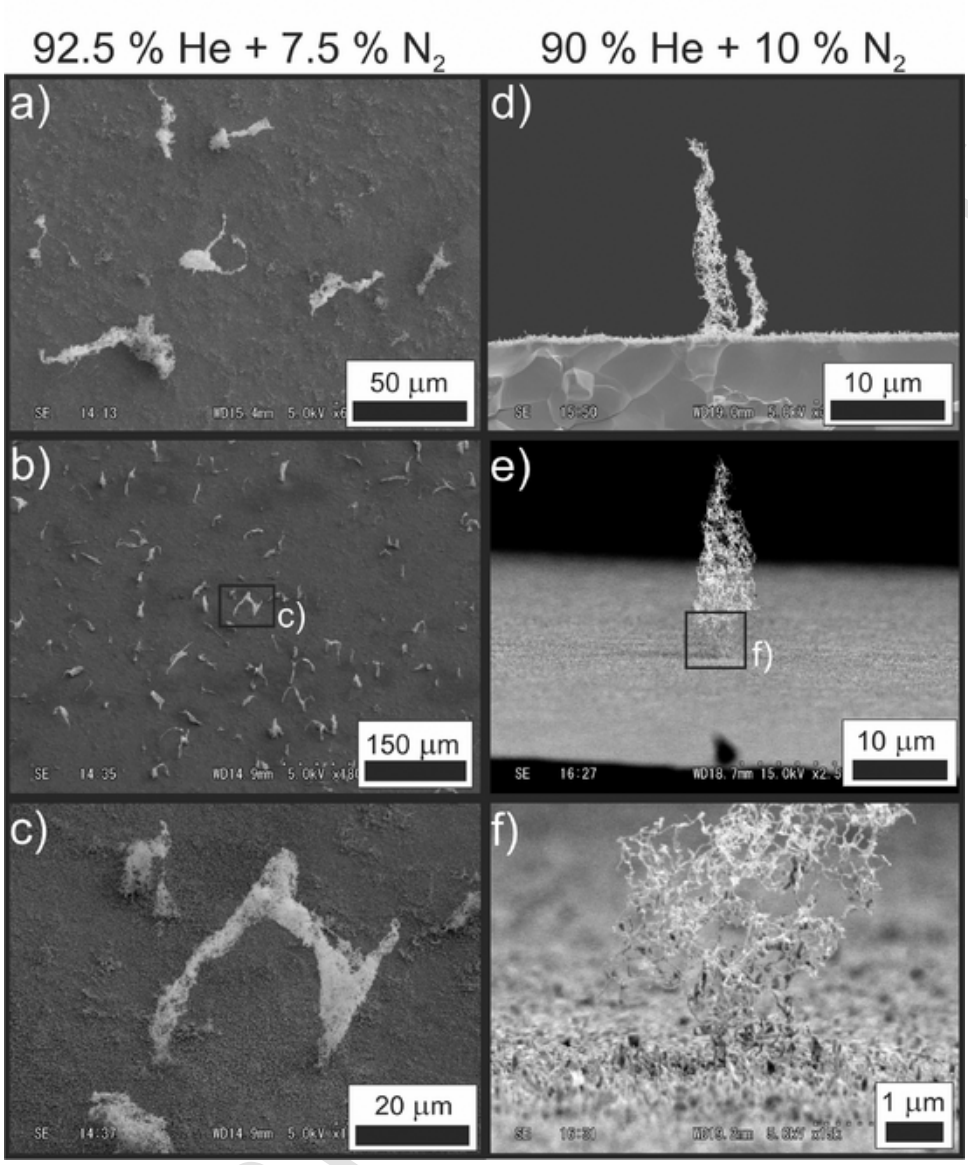

Fig. 8. Images of NTBs produced on the W surfaces exposed to He + N_2 impurity plasmas. In a), b) and c), NTBs are visible as the whitish areas on the fuzzy surface, with the grey regions representing typical fuzzy W growth. Image c) is an expanded view of the surface shown in b). In d), e) and f), NTBs are viewed at 90 and ≈ 80◦ to the surface normal, with the cross sectional thickness of the NTBs in the images estimated to be 16 – 21 μm. In f), the base of the NTB in e) is inspected closer, with the SEM imaging showing that NTBs appear to grow out of the surface they form on.

In Fig. 8d) and e), two separate NTBs were measured for the vertical heights, with the average height being found to be ≈ 20 μm. This may not be representative of all NTBs formed under a 90 % He + 10 % N_2 plasma (as not all NTBs were measured for their vertical height, and He ion fluence is known to be important for NTB growth rates [51]), but it does give an indication of the height that NTBs can grow to under these conditions. Typical fuzzy W can grow to 100s of nm to several μm depending on the exposure conditions [5], and given that the average fuzzy layer was found to be 311 ± 120 nm in thickness for the sample in Fig. 8d) and e), the NTBs have a near 70x larger vertical thickness from the surface.

Fig. 9 c) shows the results of EDX analysis for two regions (labelled in a)) on a W surface exposed to a 95 % He + 5 % N_2 sample, with spectrum 1 indicating a normal fuzz region and spectrum 2 indicating a region including an NTB on the surface. An estimation of the spatial resolution x (μm) provided by the EDX analysis is given in [52] to be,

$$x = \frac{0.064\left(E_0^{3/2} - E_c^{3/2}\right)}{\rho_w} \quad (9)$$

where E_0 is the accelerating voltage (keV), the E_c is the critical excitation energy (keV), and ρ_w is the density of the material. The density of fuzzy W layers should also be considered; it has been shown to be as low as 10 % of the bulk density [37], therefore the implantation depth may in fact be enhanced relative to bulk W. Assuming this deviation in the density, with the incident electron beam energy at 20 keV the expected depth of the EDX measurement is 0.5–5 μm. With the fuzzy layer thickness being 0.4 μm for this sample and NTBs having thicknesses from the surface of ≈ 8 μm, the penetration depth is sufficient enough to probe the typical fuzz and NTB structures.

The EDX analysis given in Fig. 9c) shows characteristic peaks for W in the spectra, indicating the two areas consist of a near identical elemental composition. Hence, the larger structures that resemble NTBs

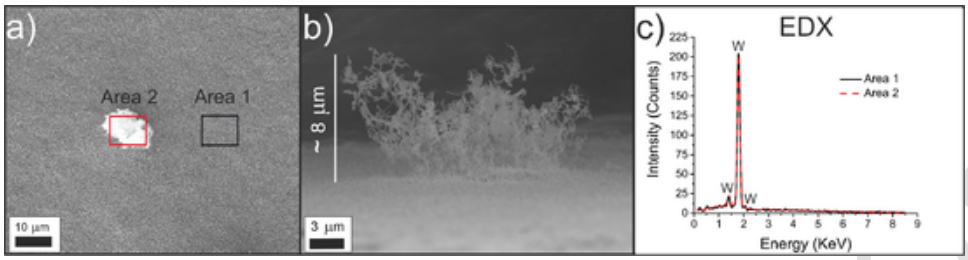

Fig. 9. Images of an NTB produced on a sample exposed to 95 % He + 5 % N_2 plasma to a total ion fluence of 1.83×10^{26} m^{-2}. In a), a top down view of the NTB is shown, in b) the NTB is viewed at ≈ 90° to the surface normal, and in c) an EDX analysis graph shows the elemental composition of the fuzzy layer (Area 1) and NTB (Area 2).

on the surface can reasonably be assumed as having a similar elemental composition to W fuzz.

4. Discussion

4.1. Mechanisms of NTB growth

In the earliest reports of "islands" of fuzzy W or NTBs in the literature [49,50,53] Woller et al. initially observed that NTBs were formed with an RF modulation of the He ion energy, varying between 25 and 100 eV [50]. A subsequent study showed that NTBs were formed at much lower frequencies of ion energy modulation (20 kHz in [49]), implying that RF modulation to the ion energy was not required to produce an NTB. In their findings, Woller et al. state the impurity % level in their device (the DIONISOS linear plasma experiment [54]) was roughly ≈ 0.1 %. Assuming the impurity type to consist of mainly air (N_2, O_2 etc), ionising these species within the He plasma could lead to larger levels of sputtering on a W surface, given the ion energy range of 25–100 eV. The reports in [49] indicate that only when a broader ion energy range distribution (from ≈ 20 to 100 eV) is used do NTBs form. At a more narrow ion energy range (≈ 50–70 eV), NTBs are not formed on the surface, but typical fuzz is formed instead.

In separate observations of NTB-like structures made by Al-Ajloni et al. in [53], a He ion beam was mixed with increasing percentages (0.01 – 0.5 %) of carbon (C). In this case the fuzz growth was near terminated at the higher percentages of C used, with small islands of fuzz (i.e. NTBs) visible on the surface when 0.01% of C was used. At the ion energies used in their study (300 eV), it is likely that with higher concentrations of C the surface sputtering rate was too large for fuzz to grow. At the lower concentrations of C, the competing processes of surface erosion and fuzz growth balance out, allowing pockets of fuzz to form on the surface.

In the investigations in [49,50,53], where fuzz growth was coupled with some low level of surface sputtering (usually by impurity species), NTBs were observed to grow on the surface. Given the previous investigations just described, it seems reasonable to assume that surface sputtering could be linked to the onset of NTB growth.

In the current study, NTBs have been observed when some small percentage (5–10%) impurity is present in the plasma. The experimental conditions chosen at the start meant that impurity ions had sufficient energy (60 eV) to sputter W. It is not yet clear how sputtering of the fuzzy W surface could lead to areas where NTBs are produced, but a possible mechanism was outlined by Hwangbo et al. in [39]. As fuzzy W formation is known to have a grain orientation dependency [55,56] and also reduce the sputtering yield from the surface, it may be that on grains where fuzzy W growth is accelerated relative to other grains, any sputtered material from the surroundings areas could be trapped (in a similar way to the line of sight deposition described in [37]) by fuzz that is already forming. As the grain orientation of tungsten surfaces was not kept constant in [39,49,53], preferential sputtering and re-deposition of fuzz could perhaps explain the formation and seemingly random distribution of NTBs on the W surfaces they form. It was shown recently how the fuzzy layer growth rate can be accelerated when fuzzy W is grown under concurrent W deposition [57–59]. McCarthy *et al* described how W deposition appears to 'match' the porosity of the surface it coalesces with [58]. The fuzzy layer thickness is then enhanced by an amount equivalent to a fully dense W layer of deposition divided by the porosity of the fuzzy surface. This implies that low levels of W deposition on to any fuzzy W surface can lead to larger fuzzy layer thicknesses. If sputtered W redeposits on a growing fuzzy layer, as may be the case in the current investigation, the large porosity of the fuzzy layer (measured to be 0.7 to 0.9 in this current work) will amount to a significant increase in the fuzzy layer when any W deposition is captured. This could be a possible explanation for the NTB growth seen here and in previous investigations.

4.2. Temperature threshold for NTB formation

In the study by Hwangbo et al. [39] a surface temperature window was observed for NTB formation. Specifically, for T_s in the range 1400 – 1600 K NTBs were formed after He + impurity exposures. The findings in this current investigation show that there is an extension to the ranges of T_s which can produce NTBs. In Fig. 10 the ranges of T_s which were observed to produce NTBs in NAGDIS-II from the study in [39] and the current investigation are shown. Also included is a temperature range observed by Woller et al. that was sufficient to produce NTBs in their experiments in [50]. It can be seen from Fig. 10 that there was a significant difference between the observed temperature range for NTBs found in [39,50]. In this current study a bridge between the two literature temperature ranges for NTB growth is approximately made, potentially expanding the temperature range for NTBs from 870 to 1600 K.

It should be noted that there was difficulty in decreasing T_s much lower than 1300 K within NAGDIS-II. Surface heating is supplied by the plasma, therefore changes to current within the plasma itself would be required, however this would in turn change the flux of particles. A cooling system can be used in NAGDIS-II to reduce T_s to temperatures as low as 1200 K, however this wasn't attempted during the experiments. In future experiments it would be useful to probe the apparent gap in the temperature range for which NTBs (in Fig. 10) can be formed.

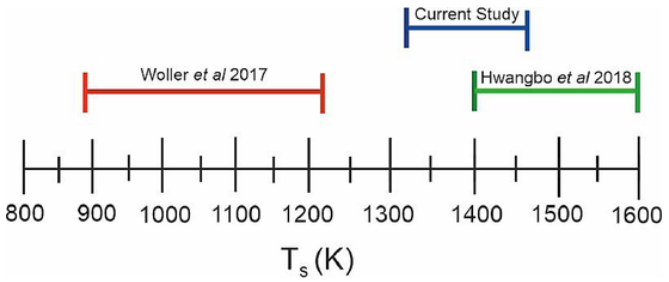

Fig. 10. Temperature range established for NTB production from the literature [39,50] and current study.

5. Conclusions

A systematic study has been carried out to find the effect of impurity species (N_2, Ne and Ar) and their concentrations (5%, 7.5% and 10%) on the effective growth rates and structures of fuzzy W produced in a high density He linear plasma device (NAGDIS-II). The effective growth rate of fuzz is reduced for impurities with higher atomic masses and higher concentrations. Mass loss measurements showed that for higher percentages of impurity in the He plasma (10%), the heavier impurity species resulted in the largest loss of mass from a fuzzy W surface, implying more sputtering had occurred. Surface microscopy revealed for N_2 (5% and 7.5%) and Ar (5%) impurity in the He plasma, W fuzz tendrils were seen. For Ne (5%, 7.5% and 10%) impurity in the He plasma, fuzzy W cones were produced. For 10% of N_2 in the He plasma, the W fuzz surface showed areas of little to no fuzz growth, with some cases of He pinholes being visible. For 7.5% and 10% of Ar in the He plasma, no fuzz was created, indicating heavy sputtering from the impurity source on the surface.

From mass loss measurements the net erosion yields were determined to decrease sharply with increasing fuzz thickness. Net erosion yields from W surfaces exposed to 95% He + 5% impurity (Ne or N_2) discharges were measured to be lower than bulk W sputtering yields for each impurity species. For long He plasma exposures (fluences up to 10^{27} m^{-2}), steady-state thicknesses of fuzz were attained due to the combined effect of fuzz growth and sputter erosion, caused by the impurity species in the plasma. The measured steady-state thicknesses were found to be consistent with an analytical model developed for the simultaneous growth and erosion of fuzz given in [6]. Over an ion fluence range from 10^{24} to 10^{27} m^{-2} and 5% of impurity in the plasma, the heavier impurity species (N_2) produced lower steady-state thicknesses of fuzz relative to the lighter species (Ne). The results here imply that using Ne would reduce the fuzzy W layer thickness at a slower rate than the heavy impurity species (N_2, Ar).

The observations of NTBs on fuzzy W surfaces were presented through SEM imaging. The formation of NTBs have been characterised in terms of their temperature threshold ranges. In this work, a temperature window of 1320–1465 K was sufficient to observe NTB formation. A possible mechanism for NTB growth through line of sight deposition and the coalescence of redeposition of sputtered W were described. Recent findings show that deposited W can match the porosity of a fuzzy W layer it lands on. This infers that W deposition could significantly enhance the fuzzy layer thickness, and may explain the onset of NTB formation. In ITER, prompt redeposition fractions will be ≈ 50% during normal operation [20], and close to 99.9% during high energy transient events [8]. As a result, significant redeposition of any sputtered wall material can occur. If NTBs are grown due to the coalescence of sputtered W and existing fuzzy tendrils, NTBs or similar larger fuzzy structures could be formed in ITER.

CRediT authorship contribution statement

Patrick McCarthy: Investigation, Data curation, Writing - original draft. **Dogyun Hwangbo:** Investigation, Data curation, Writing - review & editing. **Shin Kajita:** Supervision, Writing - review & editing. **James W. Bradley:** Conceptualization, Supervision, Writing - review & editing.

Declaration of Competing Interest

The authors declare that they have no known competing financial interests or personal relationships that could have appeared to influence the work reported in this paper.

Acknowledgements

The authors would like to thank Mr. M. Takagi for their assistance in the investigation. The authors would also like to thank the reviewers for their useful comments. P. McCarthy would like to gratefully acknowledge the Engineering and Physical Research Council (grant ref. EP/L01663X/1) for supporting this work. This work was supported in part by a Grant-in-Aid for Scientific Research 17KK0132, 19H01874 and 20K22322 from the Japan Society for the Promotion of Science (JSPS), and the NIFS Collaboration Research program.

References

[1] R.A. Pitts, S. Carpentier, F. Escourbiac, T. Hirai, V. Komarov, S. Lisgo, A.S. Kukushkin, A. Loarte, M. Merola, A.S. Naik, R. Mitteau, M. Sugihara, B. Bazylev, P.C. Stangeby, A full tungsten divertor for ITER: physics issues and design status, J. Nucl. Mater. 438 (2013) S48–S56, doi:10.1016/j.jnucmat.2013.01.008.

[2] S.E. Donnelly, The density and pressure of helium in bubbles in implanted metals: a critical review, Radiat. Effects 90 (1–2) (1985) 1–47, doi:10.1080/00337578508222514.

[3] F. Sefta, K.D. Hammond, N. Juslin, B.D. Wirth, Tungsten surface evolution by helium bubble nucleation, growth and rupture, Nucl. Fusion 53 (7) (2013) 073015, doi:10.1088/0029-5515/53/7/073015.

[4] S. Kajita, W. Sakaguchi, N. Ohno, N. Yoshida, T. Saeki, Formation process of tungsten nanostructure by the exposure to helium plasma under fusion relevant plasma conditions, Nucl. Fusion 49 (9) (2009) 095005, doi:10.1088/0029-5515/49/9/095005.

[5] M. Baldwin, R. Doerner, Helium induced nanoscopic morphology on tungsten under fusion relevant plasma conditions, Nucl. Fusion 48 (3) (2008) 035001, doi:10.1088/0029-5515/48/3/035001.

[6] T. Petty, M. Baldwin, M. Hasan, R. Doerner, J. Bradley, Tungsten "fuzz" growth re-examined: the dependence on ion fluence in non-erosive and erosive helium plasma, Nucl. Fusion 55 (9) (2015) 093033, doi:10.1088/0029-5515/55/9/093033.

[7] S. TakamuraN. OhnoD. NishijimaS. KajitaFormation of nanostructured tungsten with arborescent shape due to helium plasma irradiationPlasma Fusion Res.1200610.1585/pfr.1.051051–051

[8] G. De Temmerman, T. Hirai, R.A. Pitts, The influence of plasma-surface interaction on the performance of tungsten at the ITER divertor vertical targets, Plasma Phys. Controlled Fusion 60 (4) (2018) 044018, doi:10.1088/1361-6587/aaaf62.

[9] S. Kajita, G. De Temmerman, T. Morgan, S. van Eden, T. de Kruif, N. Ohno, Thermal response of nanostructured tungsten, Nucl. Fusion 54 (3) (2014) 033005, doi:10.1088/0029-5515/54/3/033005.

[10] M. Wirtz, M. Berger, A. Huber, A. Kreter, J. Linke, G. Pintsuk, M. Rasinski, G. Sergienko, B. Unterberg, Influence of helium induced nanostructures on the thermal shock performance of tungsten, Nucl. Mater. Energy 9 (2016) 177–180, doi:10.1016/j.nme.2016.07.002.

[11] M. Turnyanskiy, R. Neu, R. Albanese, R. Ambrosino, C. Bachmann, S. Brezinsek, T. Donne, T. Eich, G. Falchetto, G. Federici, D. Kalupin, X. Litaudon, M.L. Mayoral, D.C. McDonald, H. Reimerdes, F. Romanelli, R. Wenninger, J.H. You, European roadmap to the realization of fusion energy: mission for solution on heat-exhaust systems, Fusion Engineering and Design, 96–97, North-Holland, 2015, pp. 361–364, doi:10.1016/j.fusengdes.2015.04.041.

[12] T. Hirai, S. Panayotis, V. Barabash, C. Amzallag, F. Escourbiac, A. Durocher, M. Merola, J. Linke, T. Loewenhoff, G. Pintsuk, M. Wirtz, I. Uytdenhouwen, Use of tungsten material for the ITER divertor, Nucl. Mater. Energy 9 (2016) 616–622, doi:10.1016/j.nme.2016.07.003.

[13] D. Post, J. Abdallah, R.E. Clark, N. Putvinskaya, Calculations of energy losses due to atomic processes in tokamaks with applications to the International Thermonuclear Experimental Reactor divertor, Phys. Plasmas 2 (6) (1995) 2328–2336, doi:10.1063/1.871257.

[14] A. Kallenbach, M. Balden, R. Dux, T. Eich, C. Giroud, A. Huber, G. Maddison, M. Mayer, K. McCormick, R. Neu, T. Petrie, T. Pütterich, J. Rapp, M. Reinke, K. Schmid, J. Schweinzer, S. Wolfe, Plasma surface interactions in impurity seeded plasmas, J. Nucl. Mater. 415 (1) (2011) S19–S26, doi:10.1016/j.jnucmat.2010.11.105.

[15] R. Neu, A. Kallenbach, Overview on plasma operation with a full tungsten wall in ASDEX Upgrade, J. Nucl. Mater. 438 (2013) S34–S41, doi:10.1016/j.jnucmat.2013.01.006.

[16] A. Kallenbach, M. Bernert, T. Eich, J. Fuchs, L. Giannone, A. Herrmann, J. Schweinzer, W. Treutterer, Optimized tokamak power exhaust with double radiative feedback in ASDEX Upgrade, Nucl. Fusion 52 (12) (2012) 122003, doi:10.1088/0029-5515/52/12/122003.

[17] M. Bernert, M. Wischmeier, A. Huber, F. Reimold, B. Lipschultz, C. Lowry, S. Brezinsek, R. Dux, T. Eich, A. Kallenbach, A. Lebschy, C. Maggi, R. McDermott, T. Pütterich, S. Wiesen, Power exhaust by SOL and pedestal radiation at ASDEX Upgrade and JET, Nucl. Mater. Energy 12 (2017) 111–118, doi:10.1016/j.nme.2016.12.029.

[18] A. Kallenbach, M. Bernert, R. Dux, L. Casali, T. Eich, L. Giannone, A. Herrmann, R. McDermott, A. Mlynek, H.W. Müller, F. Reimold, J. Schweinzer, M. Sertoli, G. Tardini, W. Treutterer, E. Viezzer, R. Wenninger, M. Wischmeier, Impurity

seeding for tokamak power exhaust: from present devices via ITER to DEMO, Plasma Phys. Controlled Fusion 55 (12) (2013) 124041, doi:10.1088/0741-3335/55/12/124041.
[19] R. Wenninger, F. Arbeiter, J. Aubert, L. Aho-Mantila, R. Albanese, R. Ambrosino, C. Angioni, J.-F. Artaud, M. Bernert, E. Fable, A. Fasoli, G. Federici, J. Garcia, G. Giruzzi, F. Jenko, P. Maget, M. Mattei, F. Maviglia, E. Poli, G. Ramogida, C. Reux, M. Schneider, B. Sieglin, F. Villone, M. Wischmeier, H. Zohm, Advances in the physics basis for the European DEMO design, Nucl. Fusion 55 (2015) 063003, doi:10.1088/0029-5515/55/6/063003.
[20] G. Federici, others, C. Skinner, J. Brooks, J. Coad, C. Grisolia, A. Haasz, A. Hassanein, V. Philipps, C. Pitcher, J. Roth, W. Wampler, D. Whyte, Plasma-material interactions in current tokamaks and their implications for next step fusion reactors, Nucl. Fusion 41 (12) (2001) 1967, doi:10.1088/0029-5515/41/12/218.
[21] S. Kajita, N. Yoshida, R. Yoshihara, N. Ohno, M. Yamagiwa, TEM observation of the growth process of helium nanobubbles on tungsten: Nanostructure formation mechanism, J. Nucl. Mater. 418 (1–3) (2011) 152–158, doi:10.1016/j.jnucmat.2011.06.026.
[22] A. Khan, G. De Temmerman, T.W. Morgan, M.B. Ward, Effect of rhenium addition on tungsten fuzz formation in helium plasmas, J. Nucl. Mater. 474 (2016) 99–104, doi:10.1016/j.jnucmat.2016.03.016.
[23] R. Doerner, M. Baldwin, P. Stangeby, An equilibrium model for tungsten fuzz in an eroding plasma environment, Nucl. Fusion 51 (4) (2011) 043001, doi:10.1088/0029-5515/51/4/043001.
[24] Y. Noiri, S. Kajita, N. Ohno, Nanostructure growth by helium plasma irradiation to tungsten in sputtering regime, J. Nucl. Mater. 463 (2015) 285–288, doi:10.1016/j.jnucmat.2015.01.036.
[25] N. Ohno, D. Nishijima, S. Takamura, Y. Uesugi, M. Motoyama, N. Hattori, H. Arakawa, N. Ezumi, S. Krasheninnikov, A. Pigarov, U. Wenzel, Static and dynamic behaviour of plasma detachment in the divertor simulator experiment NAGDIS-II, Nucl. Fusion 41 (8) (2001) 1055–1065, doi:10.1088/0029-5515/41/8/309.
[26] S. Kajita, T. Yokochi, N. Ohno, T. Kumano, Near infrared radiation from heated nanostructured tungsten, Jpn. J. Appl. Phys. 51 (1) (2012) 01AJ03, doi:10.1143/JJAP.51.01AJ03.
[27] E.B. Saloman, C.J. Sansonetti, Wavelengths, energy level classifications, and energy levels for the spectrum of neutral neon, J. Phys. Chem. Reference Data 33 (4) (2004) 1113–1158, doi:10.1063/1.1797771.
[28] I. Velchev, W. Hogervorst, W. Ubachs, Precision VUV spectroscopy of Ar I at 105 nm, J. Phys. B 32 (17) (1999) L511–L516, doi:10.1088/0953-4075/32/17/105.
[29] E. Biemont, Y. Fremat, P. Quinet, Ionization potentials of atoms and ions from lithium to tin (Z = 50), At. Data Nucl. Data Tables 71 (1) (1999) 117–146, doi:10.1006/adnd.1998.0803.
[30] D.Z. Kandula, C. Gohle, T.J. Pinkert, W. Ubachs, K.S.E. Eikema, Extreme ultraviolet frequency comb metrology, Phys. Rev. Lett. 105 (6) (2010) 063001, doi:10.1103/PhysRevLett.105.063001.
[31] N. Hershkowitz, Sheaths: More complicated than think, Phys. Plasmas 12 (5) (2005) 1–11, doi:10.1063/1.1887189.
[32] W. Sakaguchi, S. Kajita, N. Ohno, M. Takagi, In situ reflectivity of tungsten mirrors under helium plasma exposure, J. Nucl. Mater. 390–391 (1) (2009) 1149–1152, doi:10.1016/j.jnucmat.2009.01.276.
[33] T. Petty, A. Khan, T. Heil, J. Bradley, Fuzzy tungsten in a magnetron sputtering device, J. Nucl. Mater. 480 (2016) 374–385, doi:10.1016/j.jnucmat.2016.08.019.
[34] R. Behrisch, W. Eckstein, Sputtering by Particle Bombardment, Topics in Applied Physics, volume 110, Springer, Berlin, Heidelberg, 2007, doi:10.1007/978-3-540-44502-9.
[35] R. Doerner, M. Baldwin, M. Simmonds, J. Yu, L. Buzi, T. Schwarz-Selinger, Quantitatively measuring the influence of helium in plasma-exposed tungsten, Nucl. Mater. Energy 12 (2017) 372–378, doi:10.1016/j.nme.2016.09.002.
[36] R. Doerner, D. Nishijima, S. Krasheninnikov, T. Schwarz-Selinger, M. Zach, Motion of W and He atoms during formation of W fuzz, Nucl. Fusion 58 (6) (2018) 066005, doi:10.1088/1741-4326/aab96a.
[37] D. Nishijima, M. Baldwin, R. Doerner, J. Yu, Sputtering properties of tungsten "fuzzy" surfaces, J. Nucl. Mater. 415 (1) (2011) S96–S99, doi:10.1016/j.jnucmat.2010.12.017.
[38] R.M. Corless, G.H. Gonnet, D.E. Hare, D.J. Jeffrey, D.E. Knuth, On the Lambert W function, Adv. Comput. Math. 5 (4) (1996) 329–359.
[39] D. Hwangbo, S. Kajita, N. Ohno, P. McCarthy, Growth of nano-tendril bundles on tungsten with impurity-rich He plasmas, Nucl. Fusion 58 (2018) 096022.
[40] W. Ni, Y. Zhang, C. Niu, Y. Cui, W. Liu, X. Li, H. Fan, G. Song, D. Liu, The effect of Ar+ impurity on W nano-fuzz growth over polycrystalline W targets, J. Nucl. Mater. 536 (2020) 152229, doi:10.1016/j.jnucmat.2020.152229.
[41] D. Nishijima, R. Doerner, D. Iwamoto, Y. Kikuchi, M. Miyamoto, M. Nagata, I. Sakuma, K. Shoda, Y. Ueda, Response of fuzzy tungsten surfaces to pulsed plasma bombardment, J. Nucl. Mater. 434 (1–3) (2013) 230–234, doi:10.1016/j.jnucmat.2012.10.042.
[42] Ä. Tanyeli, L. Marot, M.C.M. van de Sanden, G. De Temmerman, Nanostructuring of iron surfaces by low-energy helium ions, ACS Appl. Mater. Interfaces 6 (5) (2014) 3462–3468, doi:10.1021/am405624v.
[43] D. Hwangbo, S. Kawaguchi, S. Kajita, N. Ohno, Erosion of nanostructured tungsten by laser ablation, sputtering and arcing, Nucl. Mater. Energy 12 (2017) 386–391, doi:10.1016/j.nme.2017.03.004.
[44] W. Eckstein, Calculated Sputtering, Reflection and Range values, Technical Report, IPP 9/132, Max Planck Institut fuer Plasmaphysik, 2002.
[45] Y. Yao, Z. Hargitai, M. Albert, R.G. Albridge, A.V. Barnes, J.M. Gilligan, B. Pratt Ferguson, G. Lüpke, V.D. Gordon, N.H. Tolk, J.C. Tully, G. Betz, W. Husinsky, New molecular collisional interaction effect in low-energy sputtering, Phys. Rev. Lett. 81 (3) (1998) 550–553, doi:10.1103/PhysRevLett.81.550.
[46] K. Dobes, P. Naderer, N. Lachaud, C. Eisenmenger-Sittner, F. Aumayr, Sputtering of tungsten by N+ and N2+ ions: investigations of molecular effects, Phys. Scr. T145 (2011) 014017, doi:10.1088/0031-8949/2011/T145/014017.
[47] R.P. Doerner, C. Björkas, D. Nishijima, T. Schwarz-Selinger, Erosion of beryllium under high-flux plasma impact, J. Nucl. Mater. 438 (SUPPL) (2013) S272–S275, doi:10.1016/j.jnucmat.2013.01.045.
[48] R.P. Doerner, S.I. Krasheninnikov, K. Schmid, Particle-induced erosion of materials at elevated temperature, J. Appl. Phys. 95 (8) (2004) 4471–4475, doi:10.1063/1.1687038.
[49] K.B. Woller, D.G. Whyte, G.M. Wright, Isolated nano-tendril bundles on tungsten surfaces exposed to radiofrequency helium plasma, Nucl. Mater. Energy 12 (2017) 1282–1287, doi:10.1016/j.nme.2017.04.016.
[50] K. Woller, D. Whyte, G. Wright, Impact of helium ion energy modulation on tungsten surface morphology and nano-tendril growth, Nucl. Fusion 57 (6) (2017) 066005, doi:10.1088/1741-4326/aa67ac.
[51] D. Hwangbo, S. Kajita, H. Tanaka, N. Ohno, Growth process of nano-tendril bundles with sputtered tungsten, Nucl. Mater. Energy 18 (January) (2019) 250–257, doi:10.1016/j.nme.2019.01.008.
[52] J.J. Friel, X-ray and Image Analysis in Electron Microscopy, Princeton Gamma-Tech, 2004.
[53] A. Al-Ajlony, J.K. Tripathi, A. Hassanein, Role of carbon impurities on the surface morphology evolution of tungsten under high dose helium ion irradiation, J. Nucl. Mater. 466 (2015) 569–575, doi:10.1016/j.jnucmat.2015.08.036.
[54] G.M. Wright, H.A. Barnard, L.A. Kesler, E.E. Peterson, P.W. Stahle, R.M. Sullivan, D.G. Whyte, K.B. Woller, An experiment on the dynamics of ion implantation and sputtering of surfaces, Rev. Sci. Instrum. 85 (2) (2014) 023503, doi:10.1063/1.4861917.
[55] N. Ohno, Y. Hirahata, M. Yamagiwa, S. Kajita, M. Takagi, N. Yoshida, R. Yoshihara, T. Tokunaga, M. Tokitani, Influence of crystal orientation on damages of tungsten exposed to helium plasma, J. Nucl. Mater. 438 (SUPPL) (2013) S879–S882, doi:10.1016/j.jnucmat.2013.01.190.
[56] C.M. Parish, K. Wang, R.P. Doerner, M.J. Baldwin, Grain orientations and grain boundaries in tungsten nonotendril fuzz grown under divertor-like conditions, Scr. Mater. 127 (2017) 132–135, doi:10.1016/j.scriptamat.2016.09.018.
[57] S. Kajita, S. Kawaguchi, N. Ohno, N. Yoshida, Enhanced growth of large-scale nanostructures with metallic ion precipitation in helium plasmas, Sci. Rep. 8 (1) (2018) 56, doi:10.1038/s41598-017-18476-7.
[58] P. McCarthy, D. Hwangbo, M. Bilton, S. Kajita, J.W. Bradley, Enhanced fuzzy tungsten growth in the presence of tungsten deposition, Nucl. Fusion 60 (2) (2020) 026012, doi:10.1088/1741-4326/ab6060.
[59] S. Kajita, T. Morgan, H. Tanaka, Y. Hayashi, N. Yoshida, D. Nagata, J. Vernimmen, S. Feng, R. Zhang, N. Ohno, Accelerated/reduced growth of tungsten fuzz by deposition of metals, J. Nucl. Mater. 548 (2021) 152844, doi:10.1016/j.jnucmat.2021.152844.